

# Evaluation of the systematic shifts and absolute frequency measurement of a single $\text{Ca}^+$ ion frequency standard

Yao Huang · Peiliang Liu · Wu Bian ·  
Hua Guan · Kelin Gao

Received: 1 June 2013 / Accepted: 14 October 2013 / Published online: 8 November 2013  
© Springer-Verlag Berlin Heidelberg 2013

**Abstract** This paper provides a detailed description of the  $^{40}\text{Ca}^+$  optical frequency standard uncertainty evaluation and the absolute frequency measurement of the clock transition, as a summary and supplement for the published papers of Yao Huang et al. (Phys Rev A 84:053841, 1) and Huang et al. (Phys Rev A 85:030503, 2). The calculation of systematic frequency shifts, expected for a single trapped  $\text{Ca}^+$  ion optical frequency standard with a “clock” transition at 729 nm is described. There are several possible causes of systematic frequency shifts that need to be considered. In general, the frequency was measured with an uncertainty of  $10^{-15}$  level, and the overall systematic shift uncertainty was reduced to below a part in  $10^{-15}$ . Several frequency shifts were calculated for the  $\text{Ca}^+$  ion optical frequency standard, including the trap design, optical and electromagnetic fields geometry and laboratory conditions, including the temperature condition and the altitude of the  $\text{Ca}^+$  ion. And we measured the absolute frequency of the 729-nm clock transition at the  $10^{-15}$  level. An fs comb is referenced to a hydrogen maser, which is calibrated to the SI-second through the Global Positioning System (GPS). Using the GPS satellites as a link, we can calculate the frequency difference of the two hydrogen masers with a

long distance, one in WIPM (Wuhan) and the other in National Institute of Metrology (NIM, Beijing). The frequency difference of the hydrogen maser in NIM (Beijing) and the SI-second calculated by BIPM is published on the BIPM web site every 1 month, with a time interval of every 5 days. By analyzing the experimental data obtained within 32 days of a total averaging time of  $>2 \times 10^6$  s, the absolute frequency of the  $^{40}\text{Ca}^+$   $4s\ ^2S_{1/2}-3d\ ^2D_{5/2}$  clock transition is measured as 411 042 129 776 393.0 (1.6) Hz with a fractional uncertainty of  $3.9 \times 10^{-15}$ .

## 1 Introduction

Optical frequency standards have been rapidly developed thanks to recent techniques for cold atoms, optical frequency combs [3, 4] and ultra-narrow-linewidth lasers. Optical frequency standards referenced to high-Q reference transitions coupled with long interrogation times and low systematic frequency shifts are expected to take the place of the Cs primary microwave standard as the definition of the SI-second in the near future. Optical frequency standards based on ultracold neutral atoms and single ions have been developed rapidly in recent years [5–20]. Uncertainties on the order of  $10^{-17}$  or even smaller were reported with  $\text{Al}^+$ ,  $\text{Hg}^+$  and  $\text{Sr}^+$  [8, 15, 20]. The clock transition frequency had been measured by using an fs comb referenced to a Cs fountain and using Global Positioning System (GPS) as a link to the SI-second without a primary standard for direct calibration [6, 7, 9, 11–20]. As there are commercially available lasers for photo ionization, cooling, manipulation and detection, a single  $\text{Ca}^+$  ion is of several technological advantages for building a practical optical clock, which has been proposed as an alternative candidate for the next definition of the SI-second[21]. The optical

Y. Huang · P. Liu · W. Bian · H. Guan · K. Gao (✉)  
State Key Laboratory of Magnetic Resonance and Atomic and  
Molecular Physics, Wuhan Institute of Physics and Mathematics,  
Chinese Academy of Sciences, Wuhan 430071, China  
e-mail: klgao@wipm.ac.cn

Y. Huang · P. Liu · W. Bian · H. Guan · K. Gao  
Center for Cold Atom Physics, Chinese Academy of Sciences,  
Wuhan 430071, China

P. Liu · W. Bian  
Graduate School, Chinese Academy of Sciences, Beijing  
100080, China

frequency standard based on a single  $\text{Ca}^+$  ion is also being developed by the Quantum Optics and Spectroscopy Group in Innsbruck [11], the National Institute of Information and Communications (NICT) in Japan [22–24] and the Physique des Interactions Ioniques et Moléculaires in France [25].

We report on the measurements of the  $^{40}\text{Ca}^+ 4s\ ^2S_{1/2} - 3d\ ^2D_{5/2}$  transition frequency with an uncertainty level of  $10^{-15}$  using an optical frequency comb referenced to a hydrogen maser, which is calibrated through GPS as a link to the SI-second. This report presents some sources of systematic shifts which might be associated with the frequency standard and discusses future plans to optimize them. Second-order Doppler shifts, Zeeman shifts, Stark effects and the effect of gravitational potential differences between the source and the observer are all considered.

## 2 Experimental setup

In our experiment, a single  $^{40}\text{Ca}^+$  ion is produced and trapped in a miniature Paul trap within a vacuum chamber with a pressure of  $10^{-8}$  Pa level. Then, it is laser cooled to few mK. After that, the fluorescence of the  $^{40}\text{Ca}^+$  ion is collected by an imaging system, accumulated by a PMT and displayed by a photon counter. To probe the high-Q optical clock transitions, a probe laser with Hz-level linewidth is necessary. Besides, a computer-controlled laser pulses is introduced to avoid AC Stark shifts.

### 2.1 Ion-trapping and laser-cooling systems

Our experiment is implemented with a single  $^{40}\text{Ca}^+$  ion trapped and laser cooled in a miniature Paul trap (Fig. 1). The trap has an endcap-to-center distance of  $z_0 \approx 0.6$  mm with a center-to-ring electrode distance  $r_0 \approx 0.8$  mm. Two

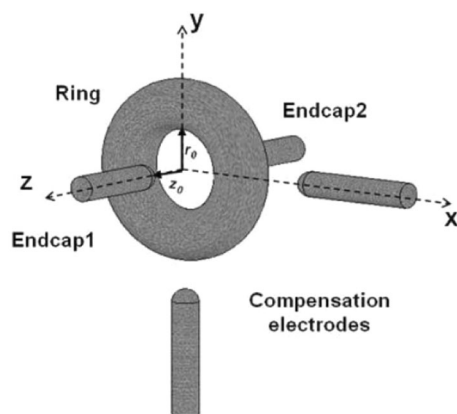


**Fig. 1** A schematic drawing of the Paul trap used in our experiments (not in scale)

electrodes perpendicular to each other are set in the ring plane to compensate the ion's excess micromotion. A trapping rf voltage of  $\sim 580$  V<sub>p-p</sub> is applied to the ring at a frequency of 9.8 MHz. The excess micromotion is nulled by applying different dc bias voltages on the endcap electrodes and the compensation electrodes. The miniature structure makes for confining a single ion in the Lamb–Dicke regime to eliminate the first-order Doppler shift; the nonstandard configuration compared with the classical Paul trap can reduce background noise.

Previously, the calcium ions were loaded by ionizing the neutral Ca-atom beam with electron bombardment. Recently, photon ionization instead of electron bombardment is used with a highly efficient loading scheme using a two-step photoionization scheme on a weak thermal beam of neutral atomic calcium [26]. The method avoids any charging of the nearby surroundings since no electron gun is used. Also, due to its extremely high efficiency, the atomic beam density can be greatly decreased, which allows one to reduce calcium deposited onto the trap electrodes from the oven.

To realize the optical frequency standard, effective trapping and cooling a single  $\text{Ca}^+$  ion steadily in a Paul trap is an important precondition. Two lasers are needed in the process of laser cooling on  $\text{Ca}^+$ . One is the 397-nm cooling laser, and the other one is the 866-nm repumping laser. The both 397- and 866-nm lasers are stabilized to the 729-nm laser using transfer cavities. The finesses of both cavities are more than 50 for the wavelengths of the diode lasers and the probe laser (729 nm). The 729-nm laser is locked to a Zerodur cavity, which has a very low drift rate, the diode lasers are coupled into two transfer cavities, respectively, together with the 729-nm laser. By scanning a PZT with a scanning frequency of 100 Hz, the transmission light of the cavities are detected by two photo diodes. By comparing the transmission fringes of the two lasers with different wavelengths, we can calculate the relative drift rate of the diode laser referenced to the 729-nm laser, and then the error signal is fed back to the diode laser to stabilize the laser frequency.

### 2.2 Ultra-narrow probe laser system

To observe the high-Q optical clock transition with a natural linewidth of 0.2 Hz, the probe laser's linewidth is expected to be at Hz level, or even sub-Hz level. A probe laser system based on a commercial Ti: sapphire laser (MBR-110, Coherent) was developed. The Ti: sapphire laser was locked to two temperature-controlled high-finesse Zerodur material Fabry–Perot cavities using Pound–Drever–Hall technique separately. The laser beam was splitted into two and locked to two individual cavities using two AOMs as actuators. Both cavities were placed on active isolated platforms

(TS-140, Table stable). A linewidth of less than 10 Hz was measured from the heterodyne beat note of the two lasers (Fig. 2). The long-term drift of the laser when locked to the cavity is  $\sim 3 \text{ Hz s}^{-1}$  using fs optical frequency comb referenced to a hydrogen maser (H-maser). An AOM (80 MHz, Brimrose) driven by a sweeping function generator (2023A, IFR) is used to compensate the long-term drift, the compensation rate is changed every 300 s to compensate the nonlinear drift. After the compensation, we got a nonlinear drift of below  $0.1 \text{ Hz s}^{-1}$ .

### 2.3 The detection of the ion spectroscopy and the probe laser locked to the clock transitions

A PMT (EMI, 9893Q/100B) collects the weak fluorescence emitted by laser-cooled  $^{40}\text{Ca}^+$  ion. The signal is amplified by a preamplifier (ORETEC, DC-200 MHz) and counted by a photon counter (Stanford Research System, SR400). The experiment processes are controlled by a personal computer program (LabVIEW 6.0). After ions are loaded in the trap, the 397-nm laser's frequency is slowly scanned across the resonance of  $4^2S_{1/2}-4^2P_{1/2}$  dipole transition, while the 866-nm laser stays at the resonance to prevent optical pumping to the  $3^2D_{3/2}$  level. Fluorescence profile of the ion is obtained.

The clock transition is observed by the electron-shelving method [27]. A pulse-light sequence is introduced to observe the clock transition spectrum in order to avoid AC Stark shift by the 397-, 866- and 854-nm radiations (Fig. 3). The pulse of the 729-nm light is about 12 ms, which induced a Fourier limit of a spectrum linewidth of  $\sim 100 \text{ Hz}$ . In the meantime, the 397-, 866-, and 854-nm lights are blocked. Then, the state of the ion is interrogated

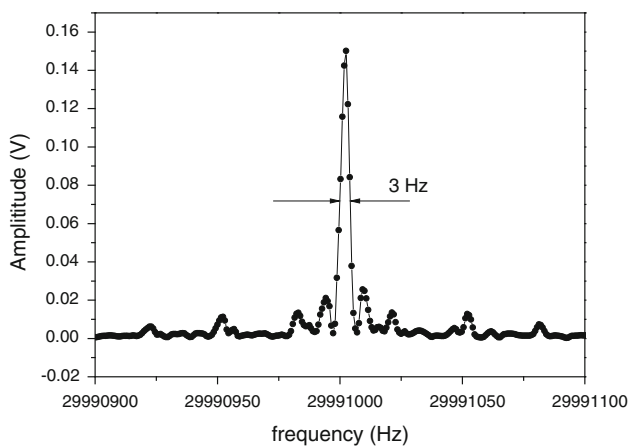


**Fig. 2** 3-Hz linewidth beat note of the Ti: sapphire laser locked to the two individual Zerodur cavities was measured using a photon detector and a spectrum analyzer (Agilent E4405B) with a resolution bandwidth of 3 Hz

using the cooling laser. If the count rate is smaller than a fixed threshold, the clock transition takes place. After the interrogation, the ion is initialized again using the 854-nm laser.

The frequency difference between the probe laser and the clock transition line center of the ion is canceled by an AOM. The required AOM frequencies are updated every 40 cycles of pulses, which cost about 1.5 s. By the “4-points locking scheme” [28, 29], three pairs of the Zeeman transitions ( $M_J = \pm 1/2$ ,  $M_J = \pm 3/2$  and  $M_J = \pm 5/2$ ) are interrogated to cancel the electric quadrupole shift [30, 31], and the offset frequency  $\Delta f(i)$  between the probe laser and the “clock” transition could be obtained every 13 s. In order to get a perfect lock, the probability of the Zeeman components which we choose are required to be equal. In practice, the magnetic field is firstly compensated to be smaller than 10 nT, which means the ten components of the Zeeman profile in all are separated by less than 800 Hz. Then, the proper angle between the direction of propagation of the laser and the direction of  $\mathbf{B}$  field is achieved by changing the current of the three pairs of coils. Finally, the polarization of the 729-nm laser beam is adjusted to get a best profile of the transitions (Fig. 4). Typically,  $\sim 150 \mu\text{W}$  of the 854-nm laser power is focused on the single ion with a spot size of  $\sim 200 \mu\text{m}$ , with a typical linewidth of 10 MHz; for the 729-nm laser, 40 nW of power with the waist of  $\sim 200 \mu\text{m}$ .

### 3 Evaluation of systematic shifts

There are a variety of potential sources of systematic shift which might be associated with the “clock” transition in a laser-cooled trapped  $\text{Ca}^+$  ion. A detailed study of the systematic offsets expected for the NIST  $\text{Hg}^+$  trap has been

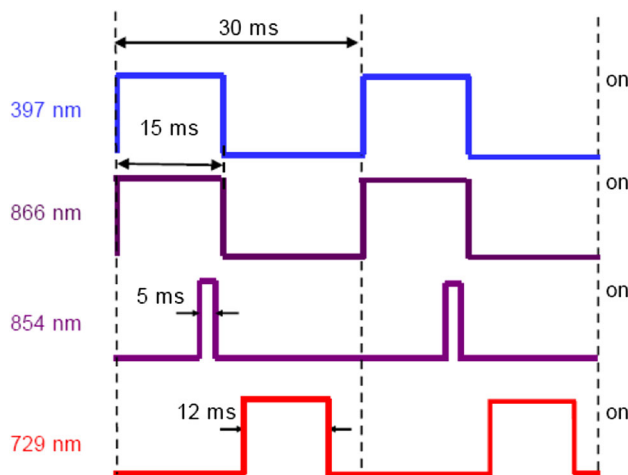


**Fig. 3** The pulse-light sequence when observing the clock transition

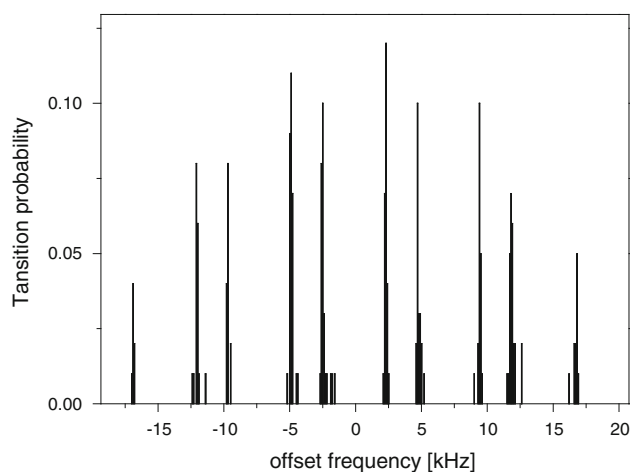


**Fig. 4** Ten components of the Zeeman profile when scanning the probe laser

published [32]. A list of expected systematic offsets for  $\text{Sr}^+$  was included in the description of the NRC frequency measurements [20, 31]. An evaluation of the systematic shifts of a  $^{43}\text{Ca}^+$  single-ion frequency standard was also made by Université de Provence [25]. And detailed reports on systematic shifts of the calcium ions had been published in our recent publications [1, 2].

Systematic effects to consider include:

- Second-order Doppler shift and Stark shift due to thermal motion
- Second-order Doppler shift and Stark shift due to micromotion
- Blackbody Stark shift
- AC Stark shift
- Zeeman fields
- Electric quadrupole shift
- Gravitational potential

In this report, we make an estimate of the above effects that are expected to give rise to frequency shifts. Under carefully controlled conditions, it should be possible to reduce all these systematic shifts to below a part in  $10^{-15}$ , that is, the sub-Hz level.

### 3.1 Second-order Doppler shift and Stark shift due to thermal motion

The second-order Doppler shift is caused by the relativistic Doppler effect, due to the ion motion relative to the laboratory frame, with bothering by the thermal kinetic energy and the micromotion. First of all, the micromotion should be minimized for achieving lower temperature and could be measured by rf-photon correlation method. After the minimization of the micromotion, we can do the measurements.

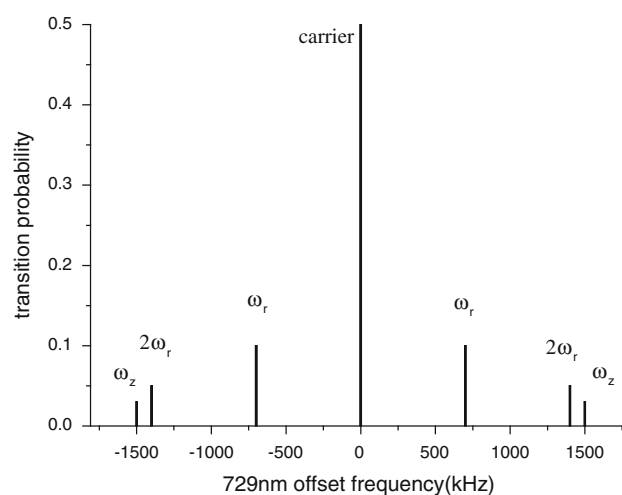


**Fig. 5** Typical secular motion sidebands and the carrier

To understand how well the ion is been laser cooled, we should estimate the ion temperature first. For our Paul trap, we measure the ion temperature by observing the intensity of secular sidebands (Fig. 5). We did measure the probability ratio for many times, and by averaging, we obtain the ratio of first sideband to carrier strength to be 0.2 (0.1).

For a single trapped ion, we can calculate the ion temperature by solving the equations [31]:

$$\left[ \frac{\sigma_1}{\sigma_0} \right]_i \cong \left( 1 + \frac{h\nu_i}{2k_B T} \right) \frac{I_1(u)}{I_0(u)} \quad (1)$$

$$u = \left( \frac{k_i^2 h}{4\pi^2 m v_i} \right) \left( \frac{k_B T}{h\nu_i} - \frac{1}{2} \right) \quad (2)$$

Thus, we obtain ion temperature of 3 (3) mK by calculation.

With the temperature estimated, we can calculate the second-order Doppler shift caused by the thermal motion using the equation [31]:

$$\left( \frac{\Delta\nu_{D2}}{\nu} \right)_{therm} = -\frac{3k_B T}{2mc^2} \quad (3)$$

in our case, the shift is calculated to be  $-4$  (3) mHz.

Thermal secular motion can push the ion out of saddle point of the trap, which introduces a Stark shift. In other words, the electric field in the ion trap has some effect changing the state energy. The Stark shift due to thermal motion can be calculated as [31]:

$$(\Delta\nu_s)_{therm} \approx \gamma_s \frac{3m\Omega^2 k_B T}{q^2} \quad (4)$$

In the above equations,  $\sigma_1/\sigma_0$  is the probability ratio of the first-order secular motion sideband and the carrier;  $h$  is the Planck constant;  $k_B$  is the Boltzmann constant;  $T$  is the ion temperature;  $\nu_i$  is the secular motion frequency;  $k_i$  is the projection of the probe laser wave vector on the  $i$  direction;

$m$  is the mass of the ion;  $I_n(u)$  is the  $n$ th order modified Bessel function.

The Stark shift rate can be calculated as:

$$\begin{aligned} \gamma_s &= \delta v / \delta E^2 \\ &= \frac{1}{h} \left\{ -\alpha_0 - \frac{1}{2} \alpha_2 (3 \cos^2 \theta - 1) \frac{[3m_j^2 - J(J+1)]}{J(2J-1)} \right\} \end{aligned} \tag{5}$$

in our case, for a single trapped  $^{40}\text{Ca}^+$ , we are measuring the frequency by averaging the frequencies of three pairs of transitions for  $m_j = 1/2, 3/2$  and  $5/2$ . Thus, the tensor part of Stark shift will be canceled. So, we only consider the scalar part by calculation [33], with the polarization rate  $\alpha_0(3d)$  is  $31.8(3) a_0^3$ , and the polarization rate  $\alpha_0(4s)$  is  $76.1(1.1) a_0^3$ , where  $a_0$  is the Bohr radius,  $a_0 \approx 0.052918$  nm, the Stark shift due to thermal motion is less than 1 mHz.

### 3.2 Second-order Doppler shift and Stark shift due to micromotion

Another relativistic effect is caused by excess micromotion. It can shift the transition line center by the relativistic Doppler effect. This shift is produced due to the ion motion relative to the laboratory frame. To estimate how much the micromotion is, we use the rf-photon correlation technique [30]. For the second-order Doppler shift caused by micromotion, it can be estimated by observing the intensity of the micromotion sidebands relative to the carrier or observing the cross-correlation signal [30]:

$$\frac{\Delta v_{D2}}{v} \approx -\frac{1}{4} \left( \frac{\gamma}{ck \cos \theta_{\mu k}} \frac{\Delta R_d}{R_{\max}} \right)^2 \tag{6}$$

where  $k$  is the wave vector,  $\Delta R_d/R_{\max}$  is the amplitude ratio of the micromotion,  $c$  is the speed of light, and  $\theta_{\mu k}$  is the angle between micromotion direction and the wave vector.

From the correlation signal observed, typically with a modulation amplitude ratio of 0.2 (0.1), considering the direction of the micromotion is not well known, the shift is estimated to be -0.02 (0.02) Hz.

The excess micromotion can push the ion out of saddle point of the trap, which introduces a Stark shift. The Stark shift due to micromotion can also be calculated from the cross-correlation signal [30]:

$$(\Delta v_s)_{\text{micro}} = \frac{1}{2} \gamma_s \left( \frac{m\gamma\Omega}{qk \cos \theta_{\mu k}} \frac{\Delta R_d}{R_{\max}} \right) \tag{7}$$

where  $k$  is the wave vector,  $\Delta R_d/R_{\max}$  is the amplitude ratio of the micromotion,  $q$  is the quantity of the electric charge, and  $\theta_{\mu k}$  is the angle between micromotion direction and the wave vector.

By calculation, our total averaged Stark shift due to micromotion is less than 1 mHz.

### 3.3 Blackbody Stark shift

There is also a Stark shift arising from blackbody radiation. The largest uncertainty in the error budget, however, stems from the AC Stark shift induced by blackbody radiation. The ion is exposed to thermal fields emanating from the surrounding vacuum vessel at room temperature. The mean-square of the frequency-dependent electric field emitted by a black body at temperature  $T$  is given by [34–36]:

$$\Delta v_{BB} = -\frac{1}{2} (831.9V/m)^2 \left( \frac{T_B(K)}{300K} \right)^4 (\alpha_0(3d) - \alpha_0(4s)) \tag{8}$$

where the  $\alpha_0(3d)$  and  $\alpha_0(4s)$  represent the scalar polarization rates for upper state and ground state, respectively. The two polarization rates have been calculated by some previous works, which can be found in Ref. [33], as described in Sect. 3.1.

In our case, at a room temperature of 293 K, assuming the real temperature fluctuation is 2 K, the shift is 0.35 (0.02) Hz.

### 3.4 AC Stark shifts

The radiations used to cool and probe the trapped ion can cause AC Stark shifts of the clock transition frequency. In our experiment, during the interrogation time, all the laser beams are switched off by mechanical shutter and AOM except for the 729-nm laser. Since this cannot be done perfectly, the residual light fields coming from stray light and incompletely switched off are expected to cause AC Stark shifts. We have measured the real efficiency of the shutter and the AOM, the shutter is better than 70 dB of the attenuation and for the AOM is better than 40 dB.

The AC Stark shift due to the laser light can be presented as [31]:

$$(\Delta v_s)_{ac} = \kappa I_0 \tag{9}$$

From the equation, we can see the AC Stark shift due to the laser light is on proportion to the laser intensity on to the ion.

For the 397-nm laser, a shutter and an AOM are used to switch off the laser beam. The frequency difference between with AOM always on and with AOM off when doing the interrogations with the 729-nm laser is measured to be less than 10 Hz. Therefore, with an attenuation of better than 40 dB for the AOM which switches off the 397-nm radiation when the measurements are made, the shift is less than 1 mHz. For the laser at 866 nm, a shutter is used to switch off the light; the frequency difference of less than 30 Hz between with shutter always on and with shutter off when doing the interrogations with

**Fig. 6** Measurement of the AC Stark shift caused by the 729-nm laser

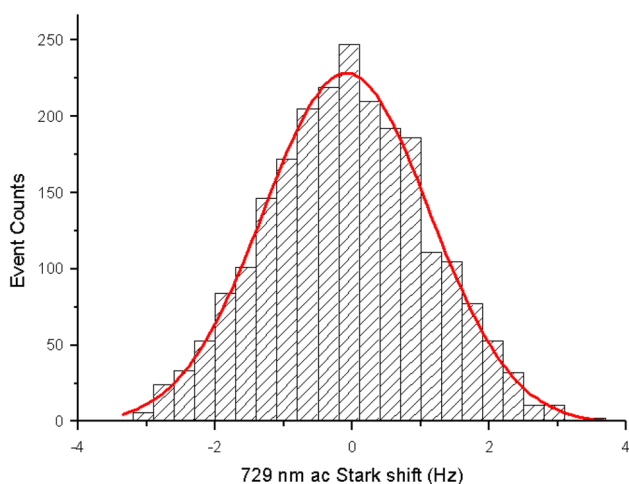
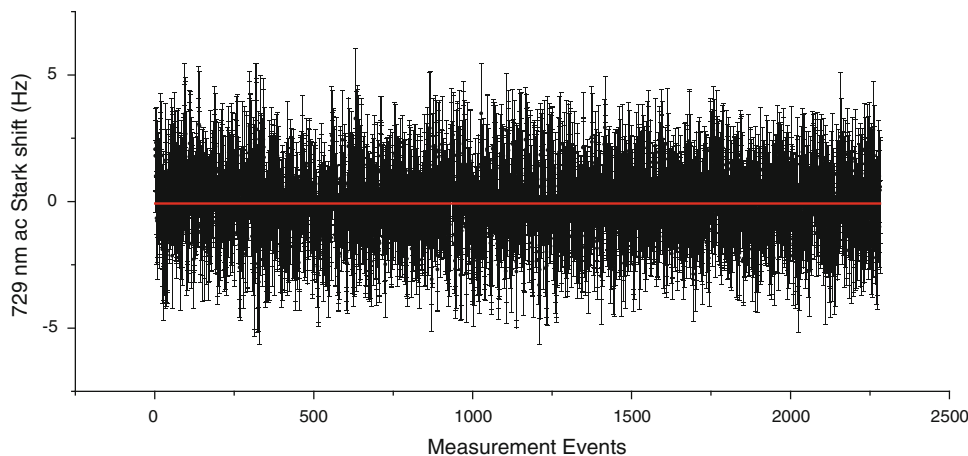


**Fig. 7** Histogram graph of the 729-nm AC Stark shift

the 729-nm laser is measured. Therefore, with an attenuation of better than 70 dB for the shutter which switches off the 866-nm radiation when the measurements are made, the shift is less than 1 mHz. For the 854-nm laser beam, two individual shutters are used to block the light. A frequency difference between with 854-nm laser off and with only one shutter off when doing the interrogations with 729-nm laser is measured to be less than 20 Hz. Therefore, with an attenuation of better than 70 dB for the other shutter which switches off the 854-nm radiation when the measurements are made, the shift should be less than 1 mHz.

The AC Stark shift caused by the 729-nm laser is measured by doing measurements at different probe laser intensities. For the AC Stark shift due to the laser light is on proportion to the laser intensity on to the ion, we simply did a linear fit and calculate the slope. We did this kind of measurements for  $\sim 2,300$  times as in Fig. 6.

We draw a histogram graph and find that the distribution is Gaussian (Fig. 7).

From the experiment results, we obtain a linear fit slope of 0.04 (0.06) Hz/I, where I is the typical intensity used for the measurements.

### 3.5 Zeeman shift

The total nuclear magnetic moment of  $\text{Ca}^+$  is zero, so there is no hyperfine structure. The two  $4s\ S_{1/2}$  ground, as well as the six  $3d\ D_{5/2}$  excited states, is shifted by the Zeeman effect in the presence of an external magnetic field. The linear frequency shift can be calculated by the following equation:

$$\Delta\nu_{\text{linz}} = m_J g_J \frac{\mu_B B}{\hbar} \quad (10)$$

The level shift of adjacent Zeeman levels is 28 Hz/nT for the ground state and 17 Hz/nT for the excited state. There is also a small quadratic contribution from coupling of the  $D_{5/2}$  sublevels with  $|m_D| \leq 3/2$  to the  $D_{3/2}$  level but it is rather small due to the fine structure splitting of 1.819 THz. The average shift over all six levels is  $\sim 1.9\ \mu\text{Hz/nT}$  in our case for  $\sim 400$  nT of magnetic field by calculation using second-order perturbation theory. The shift is given by the equation [31]:

$$\Delta\nu_{z2} = K \frac{\mu_B^2 B^2}{\hbar^2 \nu_{DD}} \quad (11)$$

which is also called the second-order Zeeman shift. Where,  $\nu_{DD}$  is the fine structure splitting and  $\hbar$  the Planck constant and  $K$  a constant depending on the magnetic sublevel given by [31]:

$$\begin{aligned} K &= \frac{6}{25}; m_J = \pm \frac{1}{2} \\ K &= \frac{4}{25}; m_J = \pm \frac{3}{2} \\ K &= 0; m_J = \pm \frac{5}{2} \end{aligned} \quad (12)$$

For a transition frequency measurement at the  $10^{-15}$  level, it is necessary to have control over the Zeeman effect. By averaging the transitions 1–6, the linear dependence on the magnetic field completely cancels because they are symmetric with respect to the line center. The error is limited by the number of measurements only. In order to calculate the statistical error for the data, the individual AOM frequencies and the respective frequency deviations were used. The laser was locked to the ion by the method described above, and its frequency can be regarded as constant over time. By statistical calculation, the linear Zeeman shift in May 2011 was 0 (0.19)Hz, and in June 2011, the shift was (0.26) Hz.

As for the second-order Zeeman shift, for our system, the average magnetic field during the measurements is 430 nT, and the fluctuation of the field we measured is about 3 nT. This leads to a second Zeeman shift of <1 mHz.

### 3.6 Electric quadrupole shift

The electric quadrupole moment of the  $D_{5/2}$  levels couples to static electric field gradients caused by either the DC-trapping fields or possible spurious field gradients of patch potentials. There will be an electric quadrupole shift due to the presence of electric field gradients, which interact with the electric quadrupole moment of the ion. However, by averaging the center frequency of the three pairs of the components, we can null the quadrupole shift [9, 31]. By averaging the difference of center frequency for different components, with statistics, Gaussian distributions are obtained (Fig. 8).

From the above figures, we can see the distribution is Gaussian, and thus, we use the Gaussian fit. By calculation, we obtain in May 2011, the shift was 0 (0.030) Hz, and in June 2011, the shift is 0 (0.021) Hz.

### 3.7 Gravitational shift

A gravitational potential difference between two clocks gives rise to a frequency difference due to general relativity effect. For earth-based clocks, the relative frequency shift is approximately given by the height difference  $\Delta h$  and the gravitational acceleration  $g$  provided the clocks are almost at the same height [37]:

$$\frac{\delta f}{f_0} = \frac{g\Delta h}{c^2} \tag{13}$$

We measured the altitude of our ion trap referenced to the sea level using GPS. The measured results were 35.2 (1.0) m, thus the gravitational shift for the clock is estimated to be 1.583 (0.045) Hz.

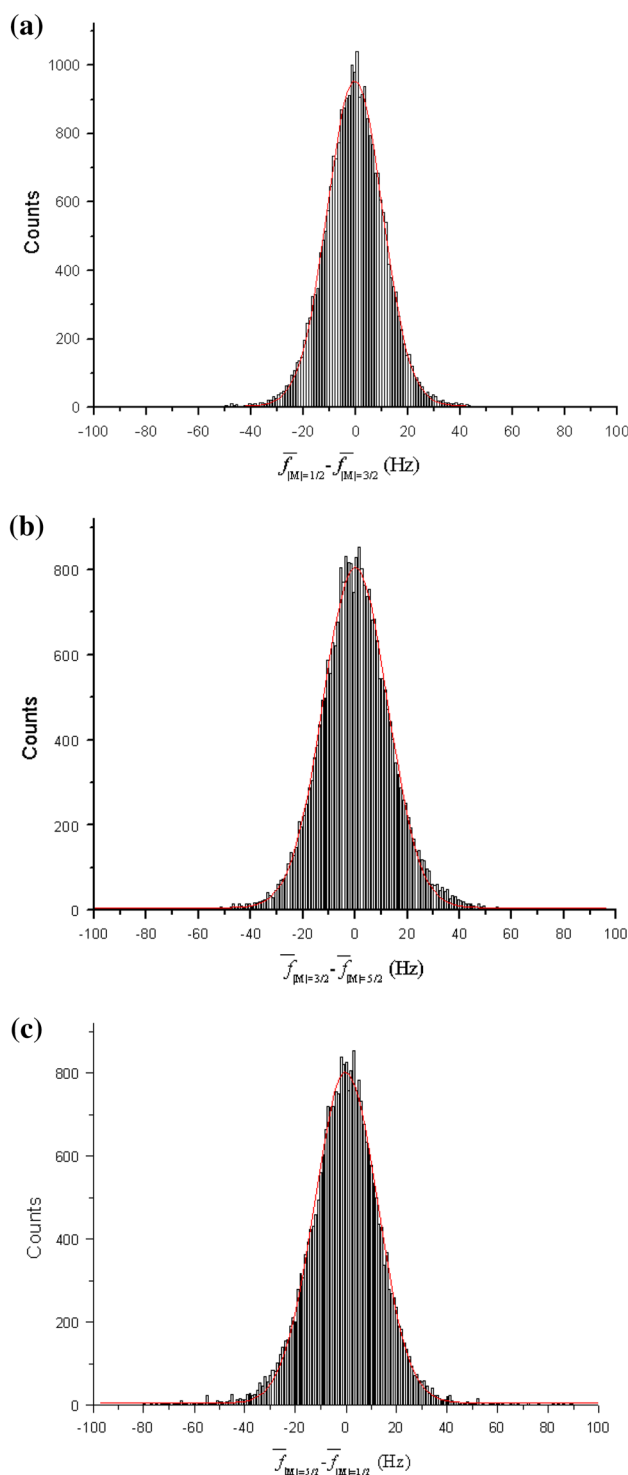


**Fig. 8** Histogram of the frequency difference of two pairs of Zeeman transitions in May 2011 **a**  $M_J = 1/2$  and  $M_J = 3/2$ , **b**  $M_J = 3/2$  and  $M_J = 5/2$ , **c**  $M_J = 5/2$  and  $M_J = 1/2$

### 3.8 Summary of the various effects

We list all significant frequency shifts in Table 1. Taking into account all of them; we get a total fractional shift of

**Table 1** The systematic frequency shifts and their uncertainties of the evaluation of the clock. Shifts and uncertainties given are in fractional frequency units ( $\Delta\nu/\nu$ )

Effect	Measurements in May		Measurements in June	
	Shift ( $10^{-16}$ )	Uncertainty ( $10^{-16}$ )	Shift ( $10^{-16}$ )	Uncertainty ( $10^{-16}$ )
Second-order Doppler shift due to thermal motion	-0.10	0.10	-0.10	0.10
Second-order Doppler shift due to micromotion	-0.49	0.49	-0.49	0.49
Stark shift due to thermal motion and micromotion	0	0.04	0	0.04
AC Stark shift due to 397 nm, 866 nm and 854 nm	0	0.04	0	0.04
AC Stark shift due to 729 nm	0.97	1.46	0.97	1.46
Blackbody radiation shift	8.51	0.27	8.51	0.27
Linear Zeeman shift	0	4.52	0	6.23
2nd Order Zeeman shift	0	0.01	0	0.01
Electric quadrupole shift	0	0.72	0	0.51
Gravitational shift	38.44	1.10	38.44	1.10
Total shift	47.4	5.0	47.4	6.5

$4.74 \times 10^{-15}$  with a fractional uncertainty of  $5.0 \times 10^{-16}$  from the data obtained in May 2011 and a total fractional shift of  $4.74 \times 10^{-15}$  with a fractional uncertainty of  $6.5 \times 10^{-16}$  for the data obtained in June 2011. We find that the uncertainty of linear Zeeman shift is in fact limiting the final systematic uncertainty. The linear Zeeman effect uncertainty is mainly caused by the fluctuation of the magnetic field, which was measured by calculating the variance of the Zeeman splitting of the Zeeman transitions. According to the variance of the Zeeman splitting, the uncertainty was calculated from statistics. To reduce the systematic uncertainties in the future, one has to increase the stability of the magnetic field.

#### 4 Measurement of the absolute frequency of the 729-nm clock transition

To measure the clock transition frequency, a fs comb was used referenced to a hydrogen maser. A commercial Ti: sapphire-based optical frequency comb (FC 8004, Menlo Systems) is used to measure the 729-nm laser frequency.

A mode-locked Ti: sapphire laser pumped by 6 W laser at 532 nm (Verdi V-6, Coherent) produce fs pulses (normally 30 fs) at a repetition rate of approximately 200 MHz. The frequency of the  $n$ -th comb component can be expressed as  $f_n = n \times f_{\text{rep}} + f_{\text{CEO}}$  [3, 4], where  $f_{\text{rep}}$  is the repetition rate of the laser pulses and  $f_{\text{CEO}}$  is the carrier-envelope offset frequency. The output is focused into two Photon Crystal Fibers (PCFs), one for the observation of the offset frequency detection and another for the probe laser measurement. The spectrum is normally broadened to over an octave after the fiber, from approximately 500–1,100 nm. A self-referencing system with an f-to-2f interferometer is introduced for the offset frequency detection. The infrared part of the broadened comb beam is separated with a dichroic mirror and frequency doubled with the SHG using a 5-mm-long KNbO<sub>3</sub> crystal and then overlapped with the green part of the broadened beam using a polarized beam splitter (PBS). The signal-to-noise ratio (S/N) of the carrier-envelope beat frequency is 40 dB at a resolution bandwidth of 300 kHz. Both the repetition frequency and the offset frequency are locked to two individual synthesizers, which are referenced to a 10 MHz signal provided by an active H-maser (CH1-75A) with an isolated splitter and a 60-m-long standard 50-Ohm coaxial cable (RG-213). The output of the comb laser from the other PCF (with frequency of  $f_n$ ) is overlapped with the probe laser at 729 nm (with frequency of  $f_c$ ) using a PBS. The beat frequency  $f_b = |f_c - f_n|$  between the probe laser and the  $n$ th comb component at 729 nm is measured by two individual frequency counters referenced to the H-maser. Normally, the S/N of the beat frequency is 30 dB at a resolution bandwidth of 300 kHz. However, sometimes the S/N of the frequency dropped to less than 28 dB during the measurement so that the readings are not reliable. We use two individual counters measuring the beat frequency simultaneously, if the difference of the readings of the two counters are more than 1 Hz, we believe the measurement is not reliable and the measurement is not taken into count. The probe laser frequency is measured every 1 s.

The probe laser frequency measured with the comb  $f_c(i)$  could be calculated using the formula  $f_c = n \times f_{\text{rep}} \pm f_{\text{CEO}} \pm f_b$ . The integer number  $n$  could be calculated using a wavemeter with an accuracy of less than 100 MHz, and the ambiguous signs could be removed by observing the sign of the variation in the beat frequency in the beat frequency while the repetition frequency or the carrier-envelope offset frequency was changed. Figure 9b shows the probe laser frequency  $f_c(i)$  measured with the comb referenced to the H-maser. The observed short-term frequency noise is mainly contributed by the H-maser through the 60-m-long cable and the 20-MHz synthesizer that was used in locking the  $f_{\text{rep}}$  to the H-maser.



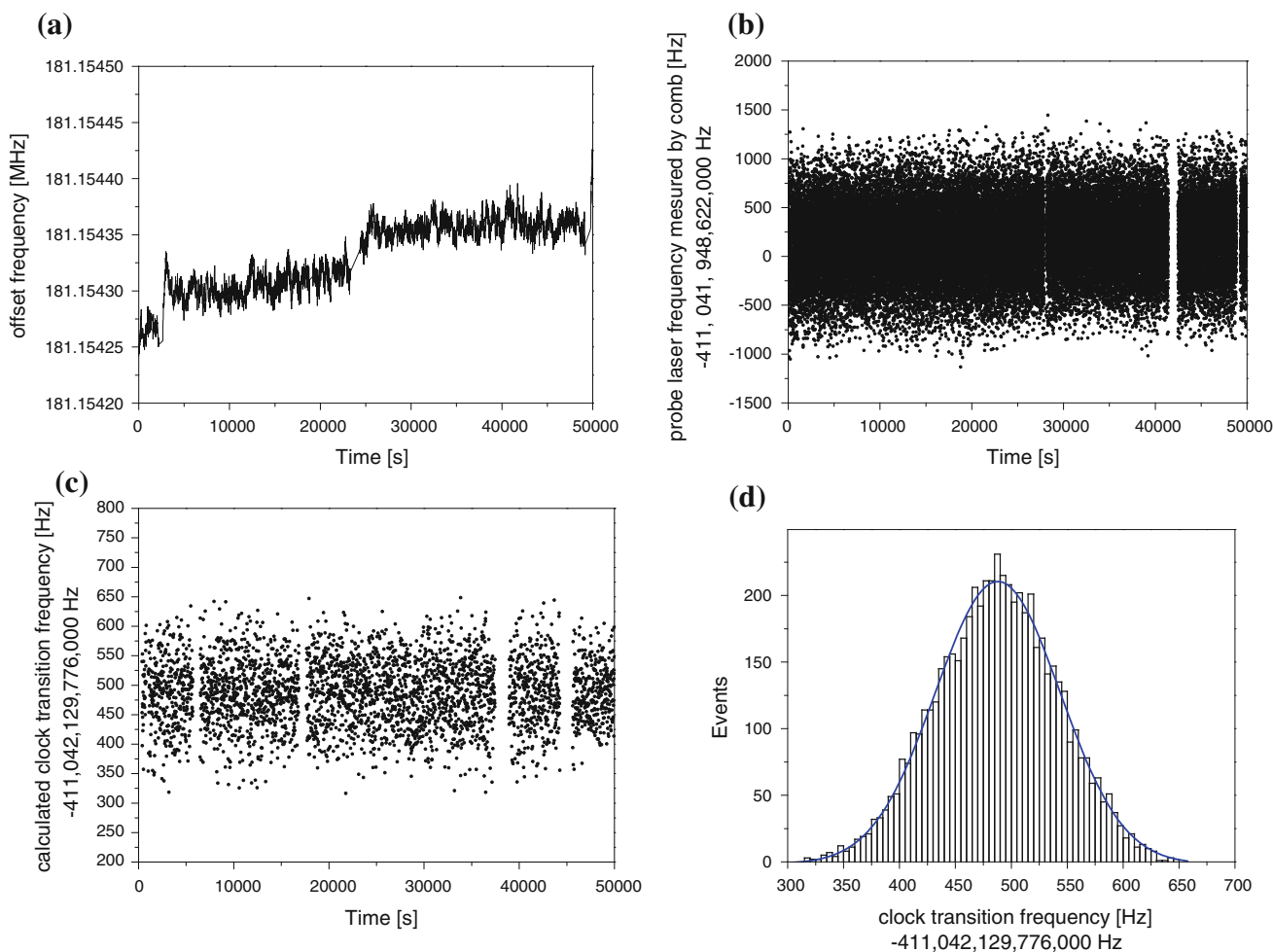


**Fig. 9** **a** Measured AOM offset frequency  $\Delta f(i)$ . **b** Measured probe laser frequency  $f_c(i)$  using the comb referenced to the H-maser. **c** Frequency of the clock transition  $\nu_0(i)$  calculated from  $\Delta f(i)$  and  $f_c(i)$ . **d** Histogram of the  $\nu_0(i)$  with a Gaussian fitting

Using the two sets of the AOM offset frequency (Fig. 9a) and the measured probe laser frequency (Fig. 9b), we calculated the clock transition frequency to be  $\nu_0(i) = f_c(i) + \Delta f(i)$  for  $i = 1, 2, \dots, i_{\max}$ , where  $i_{\max}$  represents the total measurements number. In the case showed in Fig. 9, the total measurement number is about 3500. Figure 9c shows the calculated frequency data sets of  $\nu_0(i)$ , which gives an averaged value  $\nu_0 = 411042129776490.7$  Hz. Histogram of the  $\nu_0(i)$  (Fig. 9d) follows a normal distribution; the standard deviation of the mean  $\sigma/\sqrt{i_{\max}}$  is 3.5 Hz.

With the above measurement results, we can do the measurement of the clock transition frequency referenced to the H-maser and calculate the frequency instability comparison of the  $^{40}\text{Ca}^+$  optical clock versus the H-maser (Fig. 10a). Figure 10b shows the histogram of the clock transition frequency measurements referenced to the H-maser on the day MJD 55 726, which gives an averaged value of 411 042 129 776 490.7 Hz. The histogram follows a normal distribution and the

standard deviation of the mean is 3.5 Hz. The longest continuous measurement is up to  $>50$  h. As shown in Fig. 10a, the Allan deviation for the ion transition versus the hydrogen maser comparison reaches the  $10^{-15}$  level after  $>2,000$  s of averaging time, which could be limited by the stability of the H-maser and the stability of the frequency transfer.

Frequency measurements were taken in 32 individual days, separated into two parts, one in May 2011 with 15 continuous days and the other in June 2011 with 17 continuous days (Fig. 11). Each filled circles in Fig. 11 represents a mean value of  $\nu_0(i)$  whose measurement was based directly on the H-maser. The error bars are given by the standard deviation of the mean  $\sigma/\sqrt{i_{\max}}$ . The former 15 days of measurements gives a weighted averaged frequency of 411 042 129 776 489.7 (0.9) Hz, and the later 17 days of measurements gives a weighted averaged frequency of 411 042 129 776 489.1 (0.4) Hz. The measurement described in Fig. 9 corresponds to the measurement in MJD day 55 726.

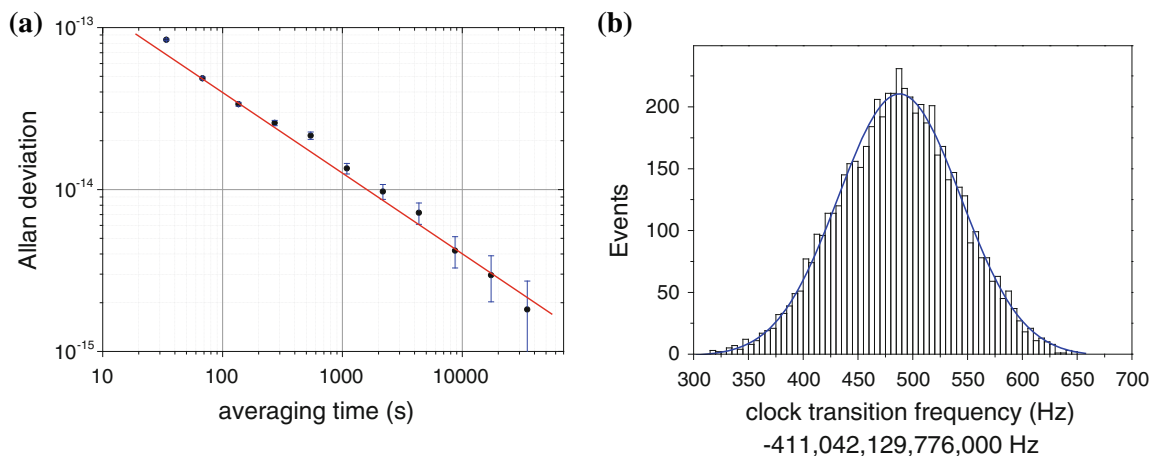
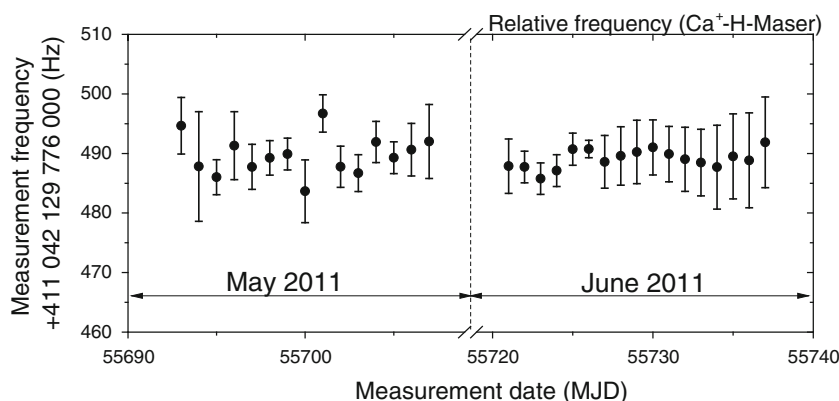


**Fig. 10** **a** The Allan deviation for the  $^{40}\text{Ca}^+$  optical clock versus the hydrogen maser, the *red line* represents  $4 \times 10^{-13} \times \tau^{-1/2}$ . **b** Histogram of the frequency measurements of the clock transition calculated

from the offset frequency and the comb measurements referenced to the H-Maser with a Gaussian fitting (*blue line*) (color figure online)

**Fig. 11** Frequency measurement of the  $4s^2S_{1/2} - 3d^2D_{5/2}$  transition of a laser-cooled trapped single  $^{40}\text{Ca}^+$  ion reference to the H-maser. *Blue solid lines* and the *red dashed lines* represent the weighted mean and the uncertainty of the frequency measurements for each month, respectively. Data shown in this figure do not include systematic corrections. Data shown in this figure do not include systematic corrections



In the first round, the laser locked to the clock transition in 1 day is about 12 h. More robustly, in the second round, the laser locked to the clock transition in 1 day is larger than 22 h. Thus, the clock in second round works for >90 % of the time, and the statistical uncertainty for 1 day of the averaging time is expected to be smaller, yet the results showed opposite. In fact, in the last 10 days, the Allan deviation only went down to  $1 \times 10^{-14}$  and then it showed a flicker floor. We think that the larger uncertainties are mainly limited by the H-Maser.

To get the final absolute frequency measurement of the clock transition, systematic shifts and the calibration of the reference must be considered and applied to the above averaged frequency. In our measurement, the largest frequency correction comes from the calibration of the frequency of the H-maser. To calibrate the frequency of the H-maser, a GPS time and frequency transfer receiver with an antenna (TTS-4, PikTime Systems) has been used. The receiver with reference to the 10 MHz and one pulse per second (pps) signals from the H-maser receives the GPS signals from 6 ~ 10 GPS satellites on average and

generates and records the GPS measurement data. In the mean time, another receiver with reference to the 10 MHz and the 1 pps signals of the UTC (NIM) in the National Institute of Metrology (NIM) of China has done a similar measurement. Using the two sets of data from the two institutes, we calculate the frequency difference of the H-maser from the UTC (NIM). Considering the frequency difference of UTC (NIM) and SI-second, the hydrogen maser we used for frequency measurement can be calibrated. Based upon the calculation with the GPS precise point-positioning (PPP) technique [38], we achieve a frequency transfer uncertainty of  $\sim 1 \times 10^{-14}$  with an averaging time of 1 day. In Fig. 12, we show the time difference between the H-maser and the UTC (NIM). The weighted average of the frequency offset between the hydrogen maser and the UTC (NIM) is then calculated to be  $-2.3649 (0.0337) \times 10^{-13}$  for the data obtained in May 2011 and  $-2.3582 (0.0083) \times 10^{-13}$  for the data obtained in June 2011 (Fig. 12).

In the mean while, the frequency difference between the UTC (NIM) and the SI-second comes from the primary

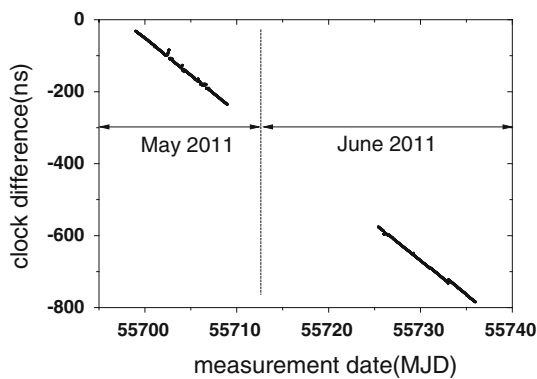


**Fig. 12** Time difference between the hydrogen maser and the UTC (NIM) calculated using PPP technique

**Table 2** The absolute frequency measurement budget table

Contributor	Measurements in May		Measurements in June	
	Shift (Hz)	Uncertainty (Hz)	Shift (Hz)	Uncertainty (Hz)
Systematic shift (Table 1)	1.95	0.21	0.95	0.27
Statistical	0	0.90	0	0.40
Hydrogen maser reference calibrated with UTC (NIM)	97.21	1.39	6.93	0.34
UTC (NIM) reference	-2.3	0.9	2.5	0.9
Total	96.9	1.9	6.4	1.1

The unit of shifts and uncertainties is given in Hz

standard can be calculated from the data reported on the BIPM web site [39]. We found the computed values of [UTC–UTC (NIM)] and uncertainties for the 2 months of our measurements in Circular T no. 281 and no. 282, the results published for the 2 months were  $0.0 (2.1) \times 10^{-15}$  in May and  $0.0 (2.1) \times 10^{-15}$  in June, respectively. We also found the estimation of the UTC accuracy by comparison of the TAI frequency with that of the given individual primary frequency standards (PFS). In these 2 months, the results published in Circular T were  $5.5 (0.3) \times 10^{-15}$  in May and  $6.0 (0.4) \times 10^{-15}$  in June. With the results of the UTC–UTC (NIM) and TAI-PFS, we calculated the frequency difference between the UTC (NIM) and the SI-second was  $5.5 (2.1) \times 10^{-15}$  for the data obtained in May 2011 and  $6.0 (2.1) \times 10^{-15}$  for the data obtained in June 2011.

Based upon the data listed in Table 2, we determine the total correction for the frequency measurement shown in Fig. 11 is  $-96.9$  Hz for the data obtained in May 2011 and  $-96.4$  Hz for the data obtained in June 2011. The combined fractional uncertainty of the absolute frequency measurement is  $4.6 \times 10^{-15}$  for the data obtained in May

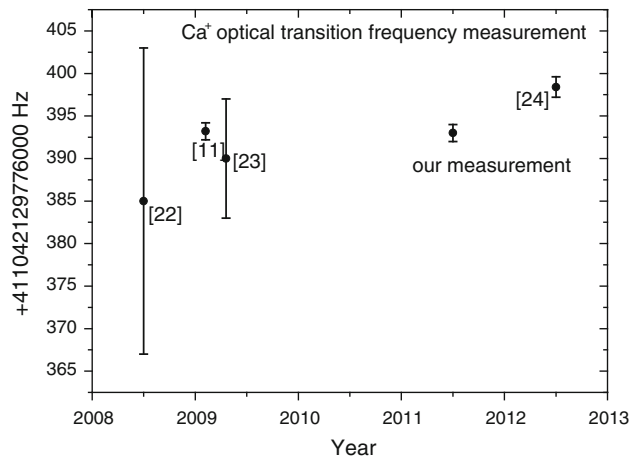


**Fig. 13** Comparison of the  $^{40}\text{Ca}^+$  clock transition frequency measured by University of Innsbruck [11], the NICT [22], [23], [24] and the results in this paper. The solid circle is the weighted mean of the data, with error bars determined by the uncertainty on the reference frequency

2011 and  $2.6 \times 10^{-15}$  for the data obtained in June 2011. The corrected absolute frequency of the  $^{40}\text{Ca}^+ 4 s^2S_{1/2}-3d^2D_{5/2}$  clock transition is 411 042 129 776 393.3 (1.9) Hz for the data obtained in May 2011 and 411 042 129 776 392.7 (1.1) Hz for the data obtained in June 2011, the two measurements agree with each other within their uncertainties. The unweighted mean of the above two values gives a final results of 411 042 129 776 393.0 (1.6) Hz, **and** the final uncertainty is calculated by considering both statistical and systematic uncertainties. The result is in agreement with the previous measurements [11, 22, 23] (Fig. 13) and the recommended frequency value [21] within their uncertainties. However, the new measurement of NICT [24] shows that a measurement difference at  $10^{-15}$  level. We will discuss the difference and do some more experiments on the systematic shifts evaluation to look for the reason.

We measure the absolute frequency of the clock transition twice: one in May 2011 and the other in June 2011; thus, we obtain two measurement results: One is 411 042 129 776 393.3 (1.9) Hz, and the other is 411 042 129 776 392.7 (1.1) Hz. The weighted mean of the above two would be 411 042 129 776 392.9 (1.0) Hz, and the unweighted mean would be 411,042,129,776,393.0 (1.6) Hz, the difference of two results is much smaller than the error, thus using any result would be fine.

We also did an evaluation on the stability of the ion clock. The “lock to ion” curve (red symbol and red line) in Fig. 14 was obtained by calculating the Allan deviation of the frequency difference between two symmetric pairs of components for the same feedback period and then divided by  $\sqrt{6}$  [40]. This factor corrects for the noise increase caused by comparing two similar signals and for the

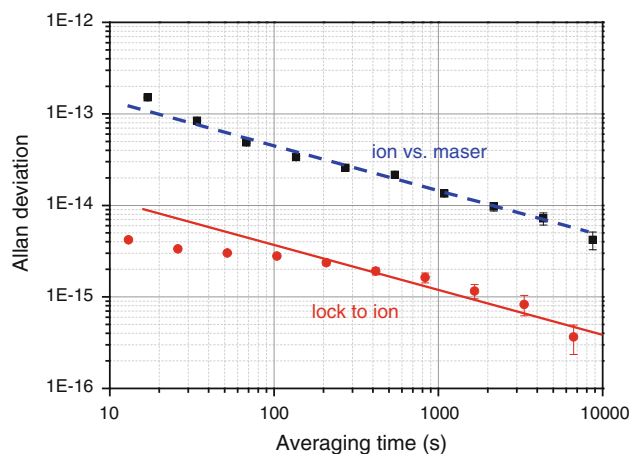


**Fig. 14** Allan deviation as a function of averaging time. The curve labeled “ion vs maser” (black symbol and blue dash line) is the Allan deviation of the hydrogen maser measured using the ion as reference. The curve labeled “lock to ion” (red symbol and red line) is the estimated Allan deviation for the lock to the ion line center (see text) (color figure online)

expected stability of the line-center data which is based on three pairs of components. For comparison, the “ion vs. maser” curve (black symbol and blue dash line) represents the Allan deviation of the comparison of the maser and the ion clock (Fig. 10a). We can see from Fig. 14 that the stability of the ion clock itself is more than ten times better than the stability of the maser. In addition to a better lock stability, state preparation will be introduced in the next step to reduce the feedback cycle by a factor of 2.

In summary, the absolute frequency measurement of the  $^{40}\text{Ca}^+ 4s^2S_{1/2}-3d^2D_{5/2}$  clock transition has been implemented at the  $10^{-15}$  level. This is a milestone toward a practical optical clock. It is important to increase the measurement precision in the precision spectroscopy research area. The better precision could be achieved if we implemented the measurement referenced to GPS as a link to the SI-second for a longer time. We shall do the comparison of the  $^{40}\text{Ca}^+$  clocks between Wuhan, Tokyo and Innsbruck, with respect to the SI-second through GPS in the future. Moreover, we suppose the stability of the hydrogen maser and the transfer cable might cause the problem of the reproducibility that is not good enough and need to be improved. By introducing cryogenic sapphire oscillators and using optical fiber as in the frequency transfer, it is possible to achieve a measurement reproducibility of  $10^{-16}$  level instead of  $10^{-15}$ . To achieve a smaller uncertainty in the future, we need to use a more stable reference such as Cs fountain instead of GPS system to achieve better results with smaller measurement uncertainty or to reduce the averaging time achieving the same uncertainty.

**Acknowledgments** We acknowledge H. Shu, H. Fan, B. Guo, Q. Liu, W. Qu, B. Ou, J. Cao and X. Huang for the early works, thank G.

Huang for his valuable suggestion, thank T. Li and K. Liang for the GPS comparison works, and thank J. Ye, F.-L. Hong, H. Klein, K. Matsubara, M. Kajita, Y. Li, P. Dubé, L. Ma, Z. Yan and C. Lee for their fruitful discussions. This work is supported by the National Basic Research Program of China (2005CB724502) and (2012CB821301), the National Natural Science Foundation of China (10874205, 10274093 and 11034009) and Chinese Academy of Sciences.

## References

1. Y. Huang, Q. Liu, J. Cao, B. Ou, P. Liu, H. Guan, X. Huang, K. Gao, *Phys. Rev. A* **84**, 053841 (2011)
2. Y. Huang, J. Cao, P. Liu, K. Liang, B. Ou, H. Guan, X. Huang, T. Li, K. Gao, *Phys. Rev. A* **85**, 030503 (2012)
3. T. Udem, T.W. Hänsch, *Nature* **416**, 233 (2002)
4. S.T. Cundiff, J. Ye, *Rev. Mod. Phys.* **75**, 325 (2003)
5. G.K. Campbell, A.D. Ludlow, S. Blatt, J.W. Thomsen, M.J. Martin, M.H.G. de Miranda, T. Zelevinsky, M.M. Boyd, J. Ye, S.A. Diddams, T.P. Heavner, T.E. Parker, S.R. Jefferts, *Metrologia* **45**, 539 (2008)
6. A.D. Ludlow, T. Zelevinsky, G.K. Campbell, S. Blatt, M.M. Boyd, M.H.G. de Miranda, M.J. Martin, J.W. Thomsen, S.M. Foreman, J. Ye, T.M. Fortier, J.E. Stalnaker, S.A. Diddams, Y. Le Coq, Z.W. Barber, N. Poli, N.D. Lemke, K.M. Beck, C.W. Oates, *Science* **319**, 1805 (2008)
7. N.D. Lemke, A.D. Ludlow, Z.W. Barber, T.M. Fortier, S.A. Diddams, Y. Jiang, S.R. Jefferts, T.P. Heavner, T.E. Parker, C.W. Oates, *Phys. Rev. Lett.* **103**, 063001 (2009)
8. C.W. Chou, D.B. Hume, J.C.J. Koelemeij, D.J. Wineland, T. Rosenband, *Phys. Rev. Lett.* **104**, 070802 (2010)
9. H.S. Margolis, G.P. Barwood, G. Huang, H.A. Klein, S.N. Lea, K. Szymaniec, P. Gill, *Science* **306**, 1355 (2004)
10. T. Schneider, E. Peik, C. Tamm, *Phys. Rev. Lett.* **94**, 230801 (2005)
11. M. Chwalla, J. Benhelm, K. Kim, G. Kirchmair, T. Monz, M. Riebe, P. Schindler, A.S. Villar, W. Hänsel, C.F. Roos, R. Blatt, M. Abgrall, G. Santarelli, G.D. Rovera, Ph Laurent, *Phys. Rev. Lett.* **102**, 023002 (2009)
12. T. Akatsuka, M. Takamoto, H. Katori, *Nat. Phys.* **4**, 954 (2008)
13. N. Poli, Z.W. Barber, N.D. Lemke, C.W. Oates, L.S. Ma, J.E. Stalnaker, T.M. Fortier, S.A. Diddams, L. Hollberg, J.C. Bergquist, A. Brusch, S. Jefferts, T. Heavner, T. Parker, *Phys. Rev. A* **77**, 050501 (2008)
14. N. Huntemann, M. Okhapkin, B. Lipphardt, S. Weyers, C. Tamm, E. Peik, *Phys. Rev. Lett.* **108**, 090801 (2012)
15. T. Rosenband, D.B. Hume, P.O. Schmidt, C.W. Chou, A. Brusch, L. Lorini, W.H. Oskay, R.E. Drullinger, T.M. Fortier, J.E. Stalnaker, S.A. Diddams, W.C. Swann, N.R. Newbury, W.M. Itano, D.J. Wineland, J.C. Bergquist, *Science* **319**, 1808 (2008)
16. J.E. Stalnaker, S.A. Diddams, T.M. Fortier, K. Kim, L. Hollberg, J.C. Bergquist, W.M. Itano, M.J. Delany, L. Lorini, W.H. Oskay, T.P. Heavner, S.R. Jefferts, F. Levi, T.E. Parker, J. Shirley et al., *Appl. Phys. B* **89**, 167 (2007)
17. F.-L. Hong, M. Takamoto, R. Higashi, Y. Fukuyama, J. Jiang, H. Katori, *Opt. Express* **13**, 5253 (2005)
18. M. Takamoto, F.-L. Hong, R. Higashi, H. Katori, *Nature* **435**, 321 (2005)
19. S.A. King, R.M. Godun, S.A. Webster, H.S. Margolis, L.A.M. Johnson, K. Szymaniec, P.E.G. Baird, P. Gill, *New J. Phys.* **14**, 013045 (2012)
20. Alan A. Madej, Pierre Dube, Zichao Zhou, John E. Bernard, Marina Gertsvolf, *Phys. Rev. Lett.* **109**, 203002 (2012)
21. Recommendation 2(c2-2009)-(CIPM)

22. K. Matsubara et al., *Appl. Phys. Express* **1**, 067011 (2008)
23. K. Matsubara et al., Joint meeting of the European frequency and time forum and the IEEE international frequency control symposium, 1 & 2, **751** (2009)
24. K. Matsubara et al., *Opt. Express* **20**, 22034 (2012)
25. C. Champenois, M. Houssin, C. Lisowski, M. Knoop, G. Hagel, M. Vedel, F. Vedel, *Phys. Lett. A* **331**, 298 (2004)
26. S. Gulde, D. Rotter, P. Barton, F. Schmidt-Kaler, R. Blatt, W. Hogervorst, *Appl. Phys. B* **73**, 861 (2001)
27. H. Dehmelt, *IEEE Trans. Instrum. Meas.* **31**, 83 (1982)
28. G. Barwood, K. Gao, P. Gill, G. Huang, H.A. Klein, *IEEE Trans. Instrum. Meas.* **50**, 543 (2001)
29. J.E. Bernard, A.A. Madej, L. Marmet, B.G. Whitford, K.J. Siemsen, S. Cundy, *Phys. Rev. Lett.* **82**, 3228 (1999)
30. D.J. Berkeland, J.D. Miller, J.C. Bergquist, W.M. Itano, D.J. Wineland, *J. Appl. Phys.* **83**, 5025 (1998)
31. A.A. Madej, J.E. Bernard, P. Dube, L. Marmet, R.S. Windeler, *Phys. Rev. A* **70**, 012507 (2004)
32. M. Itano, *J. Res. NIST* **105**, 829 (2000)
33. M.S. Safronova, U.I. Safronova, *Phys. Rev. A* **83**, 012503 (2011)
34. B. Arora, M.S. Safronova, C.W. Clark, *Phys. Rev. A* **76**, 064501 (2007)
35. J. Mitroy, J.Y. Zhang, *Eur. Phys. J. D* **46**, 415 (2008)
36. J. Mitroy, M.S. Safronova, C.W. Clark, *J. Phys. B* **43**, 202001 (2010)
37. C.W. Chou, D.B. Hume, T. Rosenband, D.J. Wineland, *Science* **329**, 1630 (2010)
38. W. Lewandowski, W.J. Azoubib, W.J. Klepczynski, *Proc. IEEE* **87**, 163 (1999)
39. Bureau International des Poids et Mesures (BIPM), Circular T, May&June [http://www1.bipm.org/en/scientific/tai/time\\_ftp.html](http://www1.bipm.org/en/scientific/tai/time_ftp.html) (2011)
40. P. Dubé, A.A. Madej, Z. Zhou, J.E. Bernard, *Phys. Rev. A* **87**, 023806 (2013)